RESEARCH ARTICLE
doi: 10.2306/scienceasia1513-1874.2025.071

ScienceAsia 51 (4): 2025: ID 2025071: **1–9**

Synthesis of $Fe_{0.82}O$/activated carbon as a degradation membrane with efficient Fenton catalytic performance

Linlin Jiang[a,b], **Junhao Zeng**[b], **Di Zhang**[b], **Feiyan Chen**[b], **Yujian Guo**[b], **Qingming Zeng**[b,*], **Jian Zhang**[a,b,*]

[a] Department of Chemistry and Chemical Engineering, Jining University, Qufu 273100 China
[b] Shandong Engineering Research Center for High Performance Silicone Rubber, Weifang 261000 China

*Corresponding authors, e-mail: sduchemzhang@163.com

Received 28 May 2024, Accepted 20 Aug 2025
Available online 30 Aug 2025

ABSTRACT: Designing a novel Fenton catalyst as a degradation membrane is meaningful in the fields of environmental science and materials chemistry. Herein, the $Fe_{0.82}O$/activated carbon (AC) composite degradation membrane was successfully prepared by using $FeCl_3 \cdot 6H_2O$ and hydroxypropyl cellulose as raw materials. The experimental results demonstrate that $Fe_{0.82}O$/AC composite exhibits excellent photo-Fenton catalytic performance under indoor light conditions. Specifically, the photo-Fenton catalytic activity of the $Fe_{0.82}O$/AC is 2.1 times and 25.5 times higher than that of pure iron oxide and AC, respectively. Additionally, we have also prepared a $Fe_{0.82}O$/AC degradation membrane, which shows outstanding catalytic performance similar to $Fe_{0.82}O$/AC composite. Both the content of $Fe_{0.82}O$ in the $Fe_{0.82}O$/AC composite and the Fe^{2+} content in $Fe_{0.82}O$ are key factors contributing to its high catalytic performance. The excellent surface adsorption properties of $Fe_{0.82}O$/AC, along with indoor lighting, further enhance the improvement of Fenton catalytic performance.

KEYWORDS: $Fe_{0.82}O$/AC, activated carbon, Fenton, degradation membrane

INTRODUCTION

The scarcity of clear water resources is further exacerbated by water pollution. In response, a plethora of water treatment technologies have been developed. Among these, Fenton catalysis has increasingly gained attention due to its cost-effectiveness and high efficiency [1, 2]. By employing water-insoluble iron compounds as catalysts, heterogeneous Fenton catalytic technology effectively mitigates the generation of iron sludge [3]. Although nanometer-sized iron compounds exhibit higher catalytic activity compared to their bulk counterparts, they present challenges in catalyst recovery.

Iron oxides, such as Fe_2O_3, Fe_3O_4, and FeOCl, are the most extensively utilized heterogeneous Fenton catalysts [4–6]. The rate-determining step in the heterogeneous Fenton reaction is the transformation of Fe^{3+} to Fe^{2+}. Consequently, the development of Fe^{2+} doped iron oxide (FexO) and its composites has emerged as an effective strategy to enhance the catalytic efficiency of heterogeneous Fenton [7]. Adsorption and degradation constitute the two primary mechanisms through which Fenton technology addresses water pollutants [8]. Given the short lifespan of the hydroxyl radicals generated during the Fenton catalysis process, their migration distance remains very limited. Thus, augmenting the surface adsorption of pollutants on the catalyst significantly aids in boosting catalytic efficiency. Activated carbon (AC), characterized by its high specific surface area and porosity, is a carbon material that is widely employed in wastewater treatment and drinking water purification owing to its superior adsorption capabilities [9].

To elevate Fenton catalytic activity, researchers have focused on the preparation of Fe^{2+} doped iron oxide and activated carbon composites, including FexO/-graphitic carbon/N-doped biochar and FexO/biomass AC, Fe doped TiO_2 photocatalysts, etc [10–12]. These AC materials facilitate the surface adsorption of pollutants and enhance the exposure of the catalyst's active sites. Our preceding studies have also delved into the synthesis of Fe^{2+} doped Fe_2O_3/C_3N_4 nanosheets, revealing that the inclusion of Fe^{2+} promotes the decomposition of H_2O_2 to yield hydroxyl radicals [13]. However, recovering the catalyst remains a challenge due to its micro-nano dimensions. In recent years, the fabrication of heterogeneous Fenton catalysts into degradation membranes has proven to be an effective solution for circumventing secondary pollution arising from the residual presence of micro-nano catalysts in water [14]. As such, it is logical to anticipate that the amalgamation of FexO/AC with a degradation membrane holds promise as a potent photo-Fenton catalytic material.

In this manuscript, we report the successful synthesis of $Fe_{0.82}O$/AC through a straightforward one-step calcination method, utilizing $FeCl_3 \cdot 6H_2O$ and hydroxypropyl cellulose as raw materials. During the formation of AC, Fe^{3+} ions undergo partial reduction to Fe^{2+} ions, thereby accelerating the decomposition of H_2O_2 to generate hydroxyl radicals. Concurrently, the integration of natural indoor light further bolsters the Fenton catalytic performance of $Fe_{0.82}O$/AC. Moreover, to preclude the residual presence of the $Fe_{0.82}O$/AC composite in water, we have additionally engineered a degradation membrane of FexO/AC, which manifests exceptional catalytic degradation capabilities. The

study also elaborates on the impact of the $Fe_{0.82}O$ content in the $Fe_{0.82}O$/AC composite and the Fe^{2+} content in $Fe_{0.82}O$.

MATERIALS AND METHODS

Chemicals

All chemicals utilized in our experiments were acquired from Sinopharm Chemical Co., Ltd. (China) and employed without undergoing any additional purification processes.

Characterization

The crystal structures of the samples were characterized using X-ray diffraction (XRD, MiniFlex 600, Rigaku, Japan). The scanning electron microscope (SEM, SU8010, Hitachi, Japan) and transmission electron microscope (TEM, 2100F, JEM, Japan) were employed to examine the morphology of the samples. The surface areas of the samples were measured through nitrogen adsorption-desorption isotherms utilizing a N_2 adsorption-desorption apparatus (Micromeritics, ASAP2460, USA). X-ray photoelectron spectroscopy (XPS, ESCALAB250Xi, Thermo Fisher Scientific, USA) analyses were conducted at an photoelectron spectrometer. The detailed structure was investigated using a Fourier transform infrared spectroscopy (FT-IR, Bruker Tensor II, Germany), which adopts solid-state infrared testing method with a range of 400–4000cm^{-1}. The ultraviolet visible diffuse reflection of the catalyst was measured using a UV-2550 ultraviolet spectrophotometer (Cary300, Agilent, USA). Additionally, an F-4600 fluorescence spectrophotometer (Hitachi, Japan) was utilized to study the photoluminescence (PL) spectra.

Synthesis of FexO/AC composite

$FeCl_3 \cdot 6H_2O$ and cellulose with different mass ratio (1:1, 1:2 and 1:3) were mixed in water evenly, which was added into a crucible and calcined in a muffle furnace at 240 °C for 1 h. The black sample was obtained, which was washed three times by acetone. The obtained samples were marked as FexO/AC-L, FexO/AC and FexO/AC-H, where the mass ratio of FexO/AC were 1:1, 1:2 and 1:3, respectively. Meanwhile, $FeCl_3 \cdot 6H_2O$ and cellulose were calcined individually under the same conditions for comparison. The product was washed with acetone for several times.

Catalytic test method

The Fenton catalytic performance of the prepared catalyst was tested with rhodamine B as pollutant substrate. Rhodamine B solution (12.5 mg/l, 20 ml) and 100 mg of FexO/AC composite were stirred for 1 h in the dark and then be put under the indoor sunlight. Then, 0.4 ml of H_2O_2 was added and recorded as the initial time. Next, 3 ml of supernatant was taken out every 2 min, and UV-Vis spectrophotometer was used to measure the change of concentration of supernatant. The rhodamine B concentration was determined at 550 nm. The FexO/AC was dispersed in acetone to form a suspension, which was then placed between two layers of filter paper and dried to obtain the degradation membrane.

RESULTS AND DISCUSSION

Structural analysis

To analyze the crystal structure of the sample, an XRD measurement was conducted, as depicted in Fig. 1a. The sample derived from the direct calcination of ferric chloride hexahydrate is identified as FeOCl (No. 39-0612) [15]. During the calcination process, cellulose was converted into amorphous AC. The sample obtained by calcination of $FeCl_3$ and cellulose is amorphous. The FexO in FexO/AC is a composite of Fe_2O_3 and Fe_3O_4. The diffraction peaks at 31° and 44° correspond to the (220) and (311) crystal planes of Fe_3O_4, respectively [16, 17]. The presence of carbon in the composite may facilitate the reduction of Fe^{3+} to Fe^{2+} in iron oxides.

Fig. 1b shows the FT-IR spectrum of iron oxide, FexO/AC and AC. The peaks at 3450 cm^{-1} and 1600 cm^{-1} for FexO/AC and AC samples represent —OH group, indicating abundant —OH in the FexO/AC and AC. However, the surface hydroxyl groups (—OH) in iron oxide are significantly less abundant than those in FexO/AC and AC. The peak at 540 cm^{-1} in the iron oxide and FexO/AC corresponds to the Fe—O vibration mode [18]. The peak at 1378 cm^{-1} in AC represents the characteristic C—H bond, which is absent in the FexO/AC composite. This disappearance indicates a high degree of carbonization within the FexO/AC composite.

Fig. 1c presents the SEM image of the FexO/AC composite, revealing that the FexO nanoparticles are embedded within the AC matrix. The average size of the FexO particles is approximately 300 nm. Conversely, the morphology of the iron oxides is micron-sized dimensions (Fig. S1). This suggests that the presence of AC in the composite inhibits the growth of iron oxides. The morphology of AC is amorphous (Fig. S2). Fig. 1d displays the HRTEM image of the FexO/AC composite. The observed lattice spacing of 0.25 nm corresponds to the (311) crystal plane of Fe_3O_4 [19, 20].

Owing to the short migration distance and transient lifespan of free radicals, the swift adsorption of pollutant molecules onto the catalyst's surface is advantageous for enhancing the catalytic degradation efficiency. Thus, the surface area of the sample has been measured (Fig. 2a). The specific surface area of FexO/AC composite is 1.84 m^2/g, which is larger than that of iron oxides (0.94 m^2/g) and AC (0.86 m^2/g) (Fig. S3). The optical properties of the prepared samples were characterized by UV-Vis reflectance spectra,

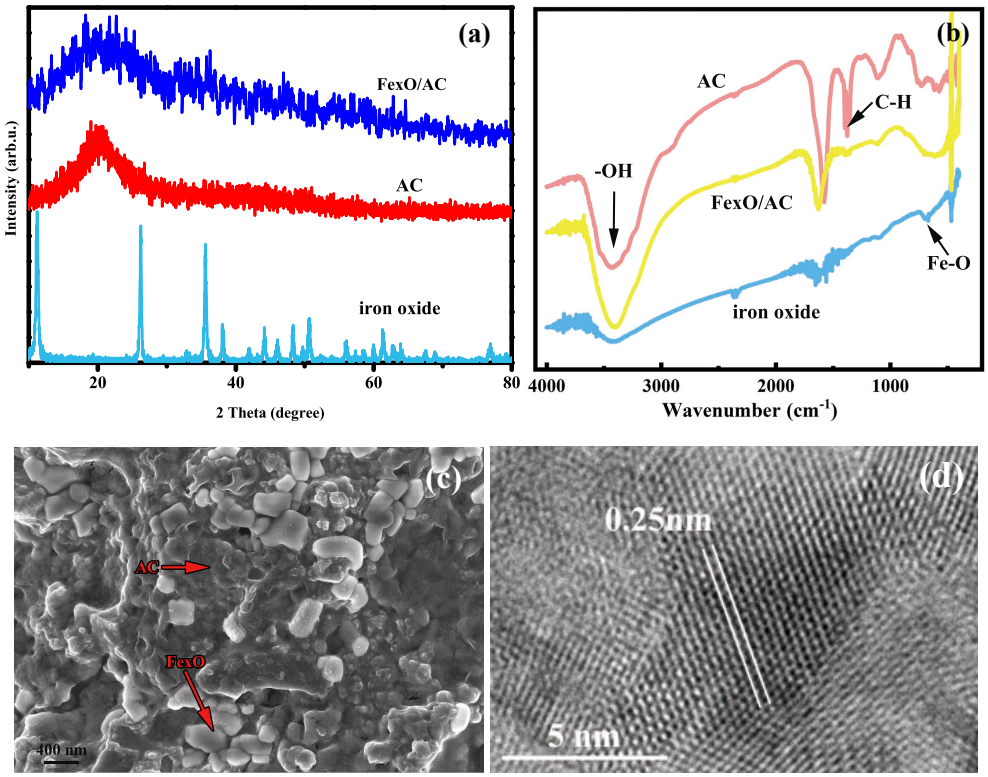

Fig. 1 (a) XRD patterns and (b) FTIR spectra of iron oxide, FexO/AC and AC, (c) SEM image and (d) TEM image of FexO/AC.

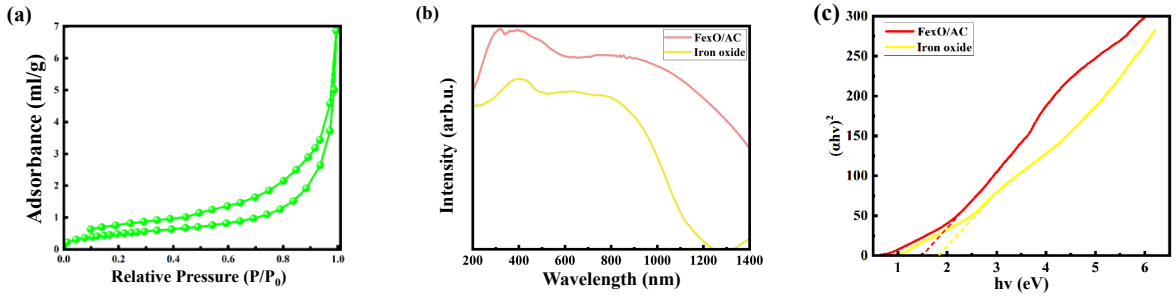

Fig. 2 (a) N_2 adsorption-desorption isotherms of FexO/AC, (b) ultraviolet-visible diffusive reflectance spectra and (c) the band gap value of iron oxide and FexO/AC.

as shown in Fig. 2b. The absorption edge band of the FexO/AC clearly shifts to a higher absorption range. The FexO/AC exhibits a broad absorption spectrum, suggesting that the FexO/AC possesses a high efficiency in utilizing solar light. According to references, the calculated optical band gap values for iron oxides and FexO/AC are 1.90 eV and 1.51 eV, respectively (Fig. 2c) [21, 22].

The XPS spectrum of the FexO/AC composite, depicted in Fig. S4, exhibits strong signals for iron (Fe), oxygen (O), and carbon (C) elements, confirming the successful integration of the two components. Fig. 3a is the Fe 2p XPS spectrum of the pure iron oxide. The Fe 2p3/2 and Fe 2p1/2 peaks locate at 710.9 eV and 724.5 eV, respectively. The peak at 718.7 eV indicates the Fe^{3+} state in the iron oxide [23, 24]. However, the Fe 2p XPS spectrum of FexO/AC composite in Fig. 3e distinctly differs from that of iron oxide. There are four peaks in the XPS spectrum of Fe 2p in Fig. 3e, which are 710.3 eV, 714.2 eV, 718.7 eV and 723.7 eV, respectively. The peaks at 710.3 eV and 718.7 eV are the characteristic peaks of Fe^{2+} [25, 26], which are consistent with the results in Fig. 1a. Meanwhile, the significantly reduced peak values of Fe 2p3/2 and Fe 2p1/2 in FexO/AC compared with iron oxide further indicates the partial reduction of iron ions [27, 28].

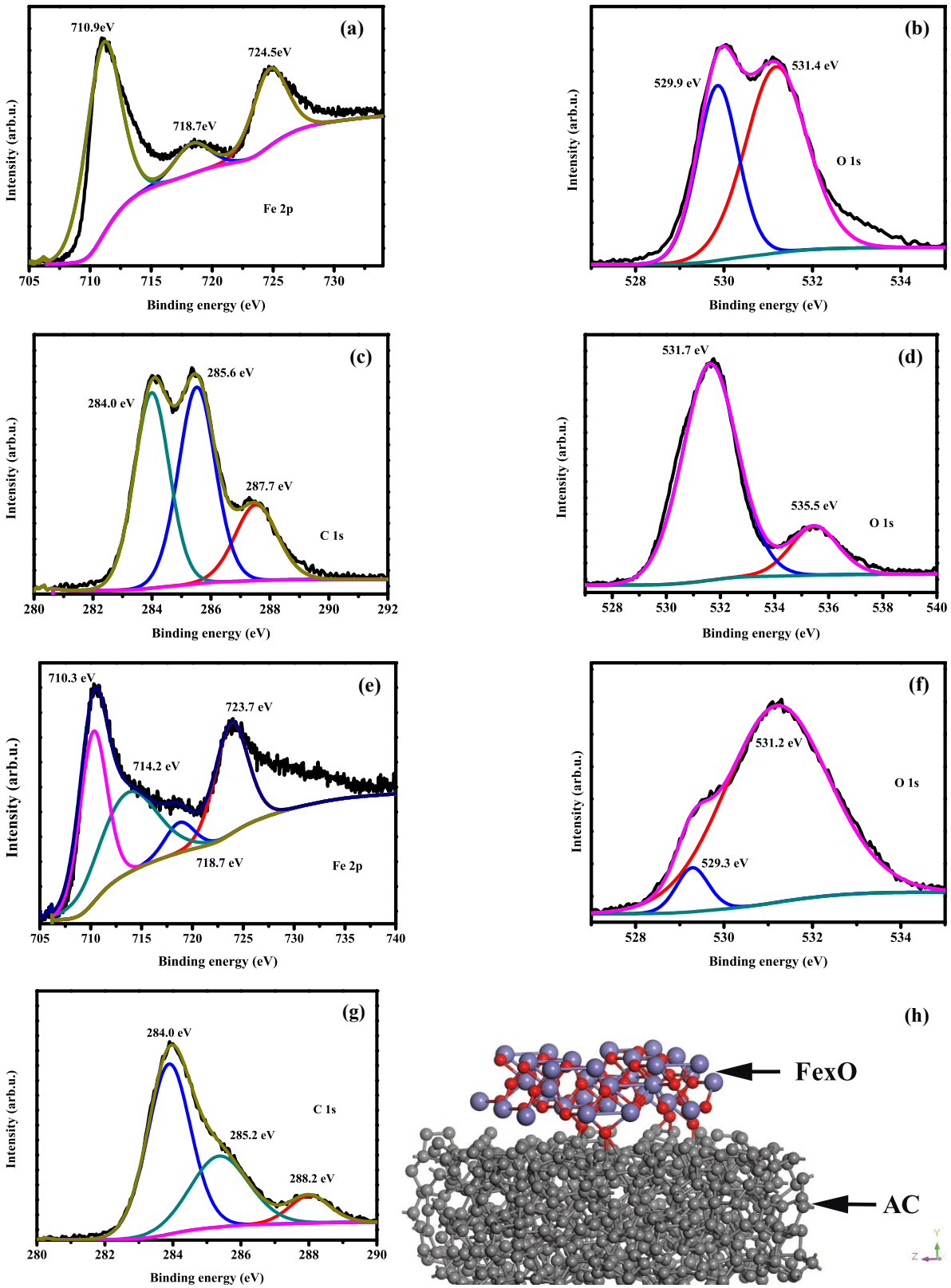

Fig. 3 XPS spectra of (a) Fe 2p and (b) O 1s in iron oxide, (c) C 1s and (d) O 1s in AC, (e) Fe 2p, (f) O 1s and (g) C 1s in FexO/AC composite, (h) schematic diagram of FexO/AC composite.

According to the XPS calculations, the content of Fe^{2+} in the FexO/AC is 56%. Thus, the x in FexO/AC should be 0.82 ($Fe_{0.82}O$/AC). The presence of Fe^{2+} in the FexO/AC could be advantageous for promoting the production of hydroxyl (·OH) radicals.

The O1s spectra of iron ions, shown in Fig. 3b, exhibit two peaks at 529.9 eV and 531.4 eV, which are attributed to Fe—O bonds and hydroxyl oxygen, respectively. The O1s spectra of the FexO/AC composite in Fig. 3f demonstrate decreased peak values at 529.3 eV and 531.2 eV. This shift is due to the presence of AC in the composite, leading to an increased content of hydroxyl oxygen in FexO/AC. In contrast, the pure AC displays O1s peaks at 531.7 eV and 535.5 eV, as seen in Fig. 3d. The peak at 535.5 eV is associated with chemisorbed water or O_2 [29, 30]. As illustrated in Fig. 3c, the C1s spectra in AC can be deconvoluted into three peaks at 284.0 eV, 285.6 eV, and 287.7 eV, signifying the presence of C—C, C—H, and C—O bonds, respectively. The C1s peaks in the FexO/AC composite are located at 284.0 eV, 285.2 eV, and 288.2 eV, as observed in Fig. 3g. A comparison between Fig. 3c and Fig. 3g reveals a noticeable decrease in the content of C—H and C—O in the FexO/AC composite. As depicted in Fig. 3h, the FexO nanoparticles are embedded within the AC matrix, creating an interface structure composed of —Fe—O—C— bonds. The presence of AC in the composite facilitates the reduction of Fe^{3+} to Fe^{2+} and inhibits the crystal growth of iron oxide.

Fenton catalytic performance

The Fenton catalytic performance was evaluated using Rhodamine B (RhB) as a model pollutant under neutral solution conditions (pH 7) and indoor lighting. Fig. 4a illustrates the Fenton catalytic activities of iron oxide, FexO/AC-L, FexO/AC-H, and AC. It can be observed from Fig. 4a that AC exhibits the weakest Fenton catalytic activity among these samples. The degradation rate of AC remains almost unchanged over 14 min, suggesting that AC primarily functions through adsorption. Both FexO/AC-L and $Fe_{0.82}O$/AC display higher Fenton catalytic activities than iron oxide, indicating that the composite structure of FexO and AC enhances the Fenton catalytic performance. However, the Fenton catalytic activity of FexO/AC-H is inferior to that of iron oxide, further confirming that AC predominantly contributes to adsorption during the catalytic process. The corresponding kinetic plots of these samples are also depicted in Fig. 4b. The degradation constants (k) of the iron oxide, FexO/AC-L, $Fe_{0.82}O$/AC, FexO/AC-H and AC are 0.24 min^{-1}, 0.49 min^{-1}, 0.51 min^{-1}, 0.11 min^{-1} and 0.02 min^{-1}, respectively. The photo-Fenton catalytic activity of the $Fe_{0.82}O$/AC composite is enhanced by factors of 2.1 and 25.5 compared to that of pure iron oxide and AC, respectively.

Under indoor lighting conditions (Fig. 4c), the degradation rate of $Fe_{0.82}O$/AC achieved 96% after 6 min. In contrast, the Fenton degradation rate under dark conditions reached 83.5% after 6 min, which is lower than that observed under indoor light. This suggests that indoor light enhances the Fenton catalytic activity. It is important to note that the photocatalytic activity of $Fe_{0.82}O$/AC under indoor light without the addition of H_2O_2 is minimal, indicating the limited photocatalytic efficiency of the $Fe_{0.82}O$/AC composite. Therefore, the role of indoor light in the degradation process is secondary.

To optimize the synthetic conditions for the $Fe_{0.82}O$/AC composite, a detailed study was conducted to examine the effects of calcination temperature and time on the Fenton catalytic activity of the resulting samples. This investigation aimed to determine the optimal parameters for achieving enhanced catalytic performance. As observed in Fig. 4d, there is a minimal difference in the Fenton catalytic activity of FexO/AC when calcined at temperatures of 220 °C, 240 °C and 260 °C. However, the calcination time has a significant impact on the catalytic activity, as shown in Fig. 4f. According to the literatures, the Fe_2O_3 can be reduced from Fe^{3+} to Fe^{2+} by carbon at high temperature, which is also closely related to the calcination time [31]. When the calcination time is short, less FexO is generated, the catalytic activity is low. When the calcination time is extended, the size of FexO in the FexO/AC composite can expand quickly. The rapid increase in particle size of FexO causes a decrease in catalytic activity. The optimal calcination time is 1 h. It can be seen from Fig. 4e that the catalytic efficiency of the $Fe_{0.82}O$/AC composite shows a trend of first increasing and then decreasing with the increase of hydrogen peroxide content. As the content of hydrogen peroxide increases from 0.1 ml to 0.4 ml, the catalytic efficiency of $Fe_{0.82}O$/AC composite does not increase significantly. However, when the amount of hydrogen peroxide increased to 0.5 ml, the catalytic efficiency significantly decreased. With the increase of H_2O_2, the generation of ·OH in the system is accelerated and the degradation efficiency is improved. Limited by the number of active sites in $Fe_{0.82}O$/AC, excess H_2O_2 cannot fully react with active sites. Besides, the produced ·OH radical can also be partially consumed by the excessive H_2O_2 [32, 33].

Performance of degradation membrane

Fig. 5a shows the schematic diagram of $Fe_{0.82}O$/AC degradation membrane and degradation unit. The $Fe_{0.82}O$/AC catalyst was bonded between two layers of filter paper, which was then placed in the filter. The H_2O_2 was added to the RhB solution, which entered the degradation membrane through a syringe. The H_2O_2 in solution was decomposed by $Fe_{0.82}O$/AC catalyst into hydroxyl radical, further realizing the degradation of RhB. Under the action of external force, the solution of RhB (12.5 mg/ml) and H_2O_2 (30% 0.4 ml) in the syringe were flowed through the $Fe_{0.82}O$/AC

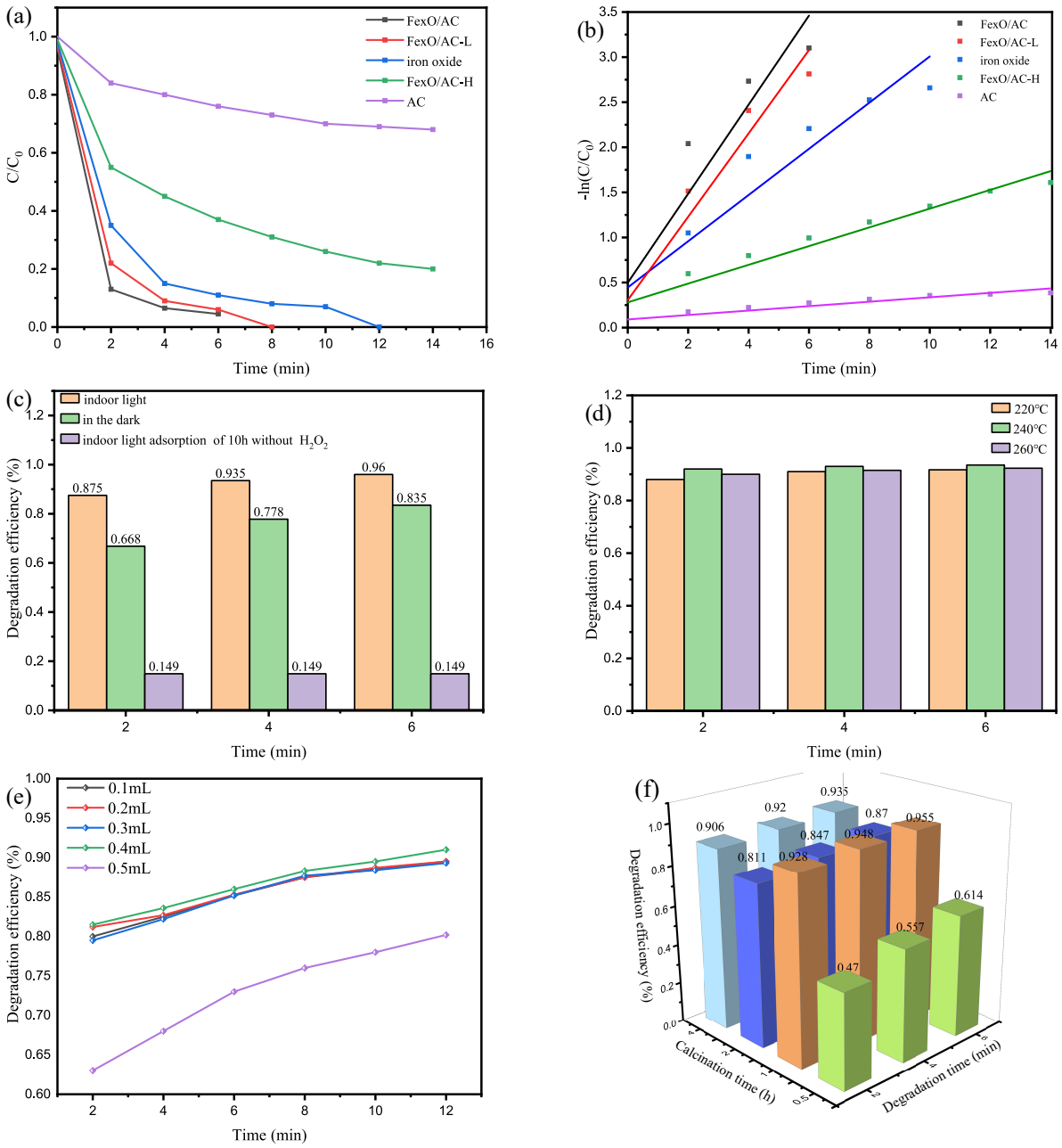

Fig. 4 (a) Catalytic degradation activity and (b) the corresponding kinetic plots of the prepared samples, (c) catalytic degradation under different light conditions and (d) calcination temperatures, (e) effect of H_2O_2 dosage and (f) different calcination time on Fenton catalytic activity.

degradation membrane. After the solution of RhB passed through the membrane, rapid degradation was achieved. It only needs to stay in the filter head for 3 s, and then RhB was dropped at the rate of 2 drops/s. In Fig. 5b, the left figure shows the degradation process without catalyst. RhB was flowed out as it was passed through the degradation membrane, indicating that the filter paper had little effect on the degradation of RhB in the device. The diameter of the used filter membrane is 50 mm. When the amount of catalyst is less than 0.15 g, that is, less than 0.76 g/cm^2, RhB cannot be completely degraded (the middle figure in Fig. 5b). When the dosage is more than 4.59 g/cm^2, the pore diameter of the catalyst is easy to be blocked, and RhB is difficult to be flowed out. Therefore, the optimal amount of catalyst is about 0.76–4.59 g/cm^2.

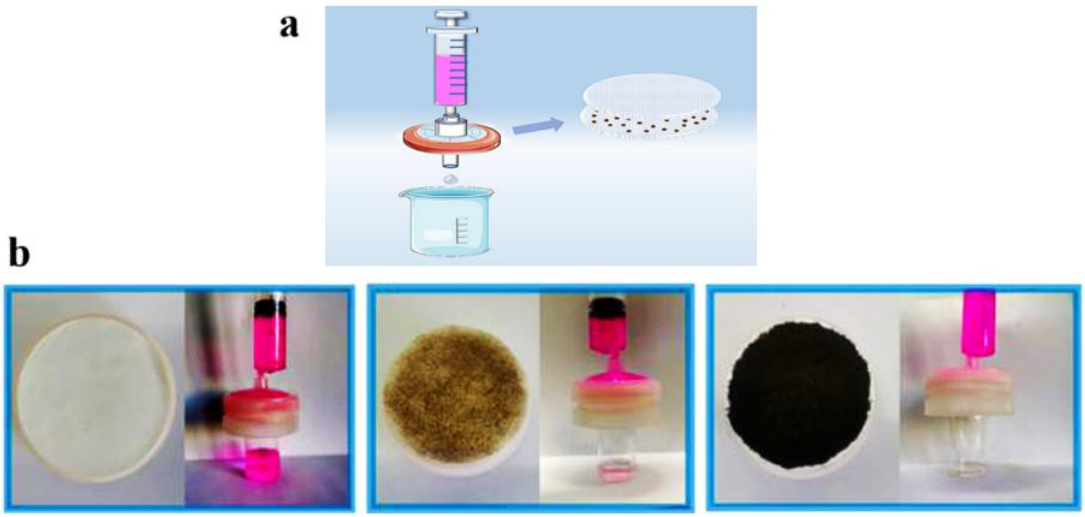

Fig. 5 (a) Schematic diagram of FexO/AC degradation membrane and degradation unit, (b) effect of different amount of FexO/AC catalyst on the degradation membrane.

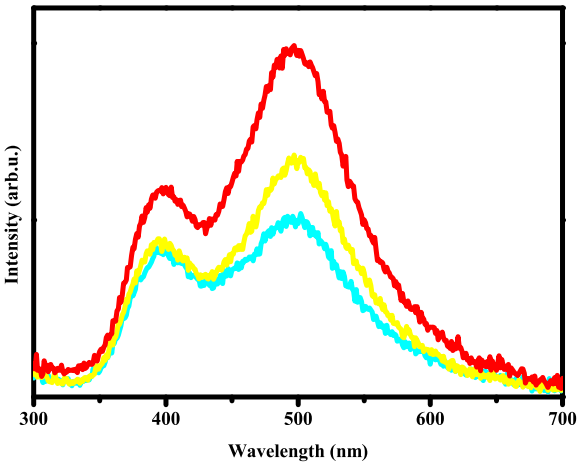

Fig. 6 Photoluminescence spectra of $Fe_{0.82}O$/AC (yellow line), FexO/AC-L (red line) and FexO/AC-H (blue line).

Catalytic mechanism

According to the results in Fig. 4, the indoor light plays a secondary role in the degradation process, while the Fenton catalysis plays a major role. In order to further study the key factors affecting the catalytic activity of $Fe_{0.82}O$/AC composite, the photoluminescence (PL) spectrum measurements have been adopted as seen in Fig. 6. The results demonstrate that the PL peak intensity of the FexO/AC is between FexO/AC-L and FexO/AC-H, which indicates that the interfacial charge transfer in $Fe_{0.82}O$/AC is also between the others. However, according to the results in Fig. 4ab, the indoor light induced photo-Fenton catalytic activity of the $Fe_{0.82}O$/AC is the highest among them. Therefore, the interfacial charge transfer is not the key reason for high photo-Fenton catalytic activity of $Fe_{0.82}O$/AC.

In addition, the specific surface area of $Fe_{0.82}O$/AC composite (1.84 m^2/g) is larger than FexO/AC-L (1.30 m^2/g) and less than FexO/AC-H (4.30 m^2/g). Although the FexO/AC-H has the biggest surface area, the Fenton catalytic activity is not the highest. The reason is that the carbon materials in the composite only have the function of adsorption but without Fenton catalytic activity. Therefore, the high specific surface area is not the key factor in high catalytic activity of the $Fe_{0.82}O$/AC composite.

As seen in Fig. 4, the catalytic activity of the$Fe_{0.82}O$/AC is the highest while that of the FexO/AC-H is the lowest among them. The low content of FexO in the FexO/AC-H is the main reason for low catalytic activity. However, the catalytic activity of the FexO/AC-L with high content of FexO is lower than that of FexO/AC. According to the XPS results, the Fe^{2+} content in FexO of FexO/AC-L is 46%, while that of $Fe_{0.82}O$/AC is 56% and that of FexO/AC-H is 21%. Thus, the Fe^{2+} content in $Fe_{0.82}O$/AC is the main reason for the high catalytic activity.

Based on the above analysis, the Fenton catalysis reaction of the $Fe_{0.82}O$/AC plays a major role in the degradation process, followed by adsorption interaction, and finally indoor light. In Fenton catalysis, the content of FexO in the $Fe_{0.82}O$/AC composite and the Fe^{2+} content in $Fe_{0.82}O$ are the key factors to determine its high catalytic performance. Additionally, a degradation membrane composed of $Fe_{0.82}O$/AC has been fabricated, demonstrating exceptional catalytic performance, which is is consistent with the results reported in the literature (such as NH_2-MIL-88B(Fe)-decorated ceramic membrane, etc.) [34].

CONCLUSION

The $Fe_{0.82}O$/AC composite has been successfully synthesized through a straightforward one-step calcination method. During this process, Fe^{3+} ions are partially reduced to Fe^{2+} ions, which enhances the production of hydroxyl radicals, thereby amplifying the catalytic activity. The Fenton catalysis reaction of the $Fe_{0.82}O$/AC composite plays a pivotal role in the degradation process.

Appendix A. Supplementary data

Supplementary data associated with this article can be found at https://dx.doi.org/10.2306/scienceasia1513-1874.2025.071.

Acknowledgements: This work was financially supported by the Science and Technology Development Plan Projects of Weifang (2022ZJ1189), Projects of 1st batch of Technology Innovation Program of Shandong Province in 2023 (202350700179), Innovation Capacity Improvement Project of Small and Medium-Sized Technology-Based Enterprise of Shandong Province (2023TSGC0706, 2023TSG C0309), Taishan Industrial Experts Program (tscy20231238).

REFERENCES

1. Brillas E (2022) Fenton, photo-Fenton, electro-Fenton, and their combined treatments for the removal of insecticides from waters and soils: A review. *Sep Purif Technol* **284**, 120290.
2. Ribeiro JP, Nunes MI (2021) Recent trends and developments in Fenton processes for industrial wastewater treatment: A critical review. *Environ Res* **197**, 110957.
3. Thomas N, Dionysiou DD, Pillai SC (2021) Heterogeneous Fenton catalysts: A review of recent advances. *J Hazard Mater* **404**, 124082.
4. Li J, You J, Wang Z, Zhao Y, Xu J, Li X, Zhang H (2022) Application of α-Fe_2O_3-based heterogeneous photo-Fenton catalyst in wastewater treatment: A review of recent advances. *J Environ Chem Eng* **10**, 108329.
5. Wang H, Zhang C, Zhang X, Wang S, Xia Z, Zeng G, Ding J, Ren N (2022) Construction of Fe_3O_4@β-CD/g-C_3N_4 nanocomposite catalyst for degradation of PCBs in wastewater through photodegradation and heterogeneous Fenton oxidation. *Chem Eng J* **429**, 132445.
6. Zhang Q, Zhang M, Li T, Du R, Yu G, Deng S (2023) FeOCl-confined activated carbon for improving intraparticle Fenton-like oxidation regeneration. *J Hazard Mater* **442**, 130026.
7. Shi L, Wang Y, Zhang C, Zhao Y, Lu C, Yin B, Yang Y, Gong X, et al (2021) An acidity-unlocked magnetic nanoplatform enables self-boosting ROS generation through upregulation of lactate for imaging-guided highly specific chemodynamic therapy. *Angew Chem Int Edit* **60**, 9562–9572.
8. Nie X, Li G, Li S, Luo Y, Luo W, Wan Q, An T (2022) Highly efficient adsorption and catalytic degradation of ciprofloxacin by a novel heterogeneous Fenton catalyst of hexapod-like pyrite nanosheets mineral clusters. *Appl Catal B Environ* **300**, 120734.
9. Azam K, Shezad N, Shafiq I, Akhter P, Akhtar F, Jamil F, Shafique S, Park YK, et al (2022) A review on activated carbon modifications for the treatment of wastewater containing anionic dyes. *Chemosphere* **306**, 135566.
10. Wang L, Guan H, Su S, Hu J, Wang Y (2022) Magnetic FeOX/biomass carbon composites with broadband microwave absorption properties. *J Alloy Compd* **903**, 163894.
11. Wang Y, Wang L, Ma F, You Y (2022) FeOx@graphitic carbon core-shell embedded in microporous N-doped biochar activated peroxydisulfate for removal of Bisphenol A: Multiple active sites induced non-radical/radical mechanism. *Chem Eng J* **438**, 135552.
12. Theerakarunwong CD, Kaewthet O, Phanichphant S (2023) Potential effectiveness of visible-light-driven Fe/TiO_2 photocatalysts for degradation of dyes contaminated wastewater and their antibacterial activity. *ScienceAsia* **49**, 454–461.
13. Shi X, Li X, Liu G, Du M, Zhang J, Liu G, Lu Q (2020) NaCl-assisted synthesis of Fe^{2+} self-doped Fe_2O_3/C_3N_4 nanosheets as efficient Fenton catalyst. *J. Mater. Sci* **55**, 10035–10046.
14. Zeng Q, Jiang Y, Ni J, Tang J, Wen Y, Fu X, Zhang Q, Xiong Z, et al (2022) Highly efficient removing refractory organics continuously using a Fenton-like Filter: The role of *in-situ* galvanic effect enhanced peroxymonosulfate activation. *Chem Eng J* **450**, 138067.
15. Wang Y, Zhang H, Zhu Y, Dai Z, Bao H, Wei Y, Cai W (2016) Au-NP-decorated crystalline FeOCl nanosheet: Facile synthesis by laser ablation in liquid and its exclusive gas sensing response to HCl at room temperature. *Adv Mater Interfaces* **3**, 1500801.
16. Wang L, Guan H, Hu J, Huang Q, Dong C, Qian W, Wang Y (2019) Jute-based porous biomass carbon composited by Fe_3O_4 nanoparticles as an excellent microwave absorber. *J Alloy Compd* **803**, 1119–1126.
17. Wang X, Liu Y, Arandiyan H, Yang H, Bai L, Mujtaba J, Wang Q, Liu S, et al (2016) Uniform Fe_3O_4 microflowers hierarchical structures assembled with porous nanoplates as superior anode materials for lithium-ion batteries. *Appl Surf Sci* **389**, 240–246.
18. Dastafkan K, Wang S, Rong C, Meyer Q, Li Y, Zhang Q, Zhao C (2022) Cosynergistic molybdate oxo-anionic modification of FeNi-based electrocatalysts for efficient oxygen evolution reaction. *Adv Funct Mater* **32**, 2107342.
19. Li W, Zhou G, Zhu X, Song M, Wang P, Ma C, Liu X, Han S, et al (2021) Magnetic assembly synthesis of high-efficiency recyclable flower-like MoS_2@Fe_3O_4@Cu_2O like-Z-scheme heterojunction towards efficient photodegradation of tetracycline. *Appl Surf Sci* **555**, 149730.
20. Yu J, Zhang T, Sun Y, Li X, Li X, Wu B, Men D, Li Y (2020) Hollow FeP/Fe_3O_4 hybrid nanoparticles on carbon nanotubes as efficient electrocatalysts for the oxygen evolution reaction. *ACS Appl Mater Inter* **12**, 12783–12792.
21. Zhao P, Ma Y, Lv X, Li M, Huang B, Dai Y (2018) Two-dimensional III2–VI3 materials: Promising photocatalysts for overall water splitting under infrared light spectrum. *Nano Energy* **51**, 533–538.
22. Tan HL, Abdi FF, Ng YH (2019) Heterogeneous photocatalysts: An overview of classic and modern approaches for optical, electronic, and charge dynamics evaluation. *Chem Soc Rev* **48**, 1255–1271.
23. Zheng N, Li X, Yan S, Wang Q, Qiao R, Hu J, Fan J, Cao G,

et al (2020) Nano-porous hollow $Li_{0.5}La_{0.5}TiO_3$ spheres and electronic structure modulation for ultra-fast H_2S detection. *J Mater Chem A* **8**, 2376–2386.
24. Tian X, Dai J, Zhu Z, Yan Y, Huo P (2020) Designed redox ions pairs imprinted photocatalyst of Fe^{3+}@PoPD/TiO_2/HNTs for enhanced photocatalytic activity. *Mater Technol* **35**, 843–852.
25. Wan J, Wu B, Lo IMC (2020) Development of FeO/Fe_3O_4 composites with tunable properties facilitated by Fe^{2+} for phosphate removal from river water. *Chem Eng J* **388**, 124242.
26. Shang Q, Zhang L, Chen C, Tang W, Han M, Chen Q, Liu W (2022) EDTA–Fe^{2+} complex-functionalized Fe_3O_4 nanozyme as tyrosine hydroxylase mimics for the production of l-DOPA. *ACS Appl. Nano Mater* **5**, 2678–2687.
27. Yang L, Amo JML, Shadike Z, Bak SM, Bonilla F, Galceran M, Nayak PK, Buchheim JR, et al (2020) A Co- and Ni-free P_2/O_3 biphasic lithium stabilized layered oxide for sodium-ion batteries and its cycling behavior. *Adv Funct Mater* **30**, 2003364.
28. Zhao W, Zhang G, Du Y, Chen S, Fu Y, Xu F, Xiao X, Jiang W, et al (2021) Sensitive colorimetric glucose sensor by iron-based nanozymes with controllable Fe valence. *J Mater Chem B* **9**, 4726–4734.
29. Zhan T, Liu W, Teng J, Yue C, Li D, Wang S, Tan H (2019) Selective oxidation of glycerol to tartronic acid over Pt/N-doped mesoporous carbon with extra framework magnesium catalysts under base-free conditions. *Chem Commun* **55**, 2620–2623.
30. Liu F, Wang Z, Zhang H, Jin L, Chu X, Gu B, Huang H, Yang W (2019) Nitrogen, oxygen and sulfur co-doped hierarchical porous carbons toward high-performance supercapacitors by direct pyrolysis of kraft lignin. *Carbon* **149**, 105–116.
31. Wu N, Liu C, Xu D, Liu J, Liu W, Shao Q, Guo Z (2018) Enhanced electromagnetic wave absorption of three-dimensional porous Fe_3O_4/C composite flowers. *ACS Sustainable Chem Eng* **6**, 12471–12480.
32. Malik PK, Saha SK (2003) Oxidation of direct dyes with hydrogen peroxide using ferrous ion as catalyst. *Sep Purif Technol* **31**, 241–250.
33. Li W, Wang Y, Irini A (2014) Effect of pH and H_2O_2 dosage on catechol oxidation in nano-Fe_3O_4 catalyzing UV-Fenton and identification of reactive oxygen species. *Chem. Eng. J* **244**, 1–8.
34. Ye Z, Oriol R, Yang C, Sirés I, Li X (2022) A novel NH_2-MIL-88B(Fe) modified ceramic membrane for the integration of electro-Fenton and filtration processes: A case study on naproxen degradation. *Chem Eng J* **433**, 133547.

Appendix A. Supplementary data

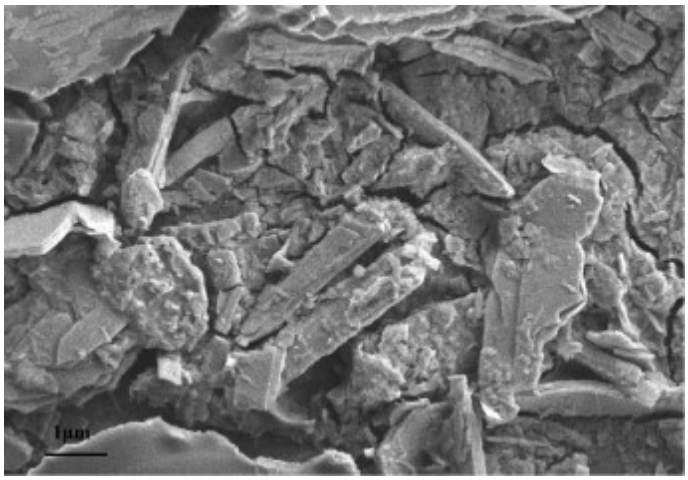

Fig. S1 The morphology of iron oxide as analysed by SEM.

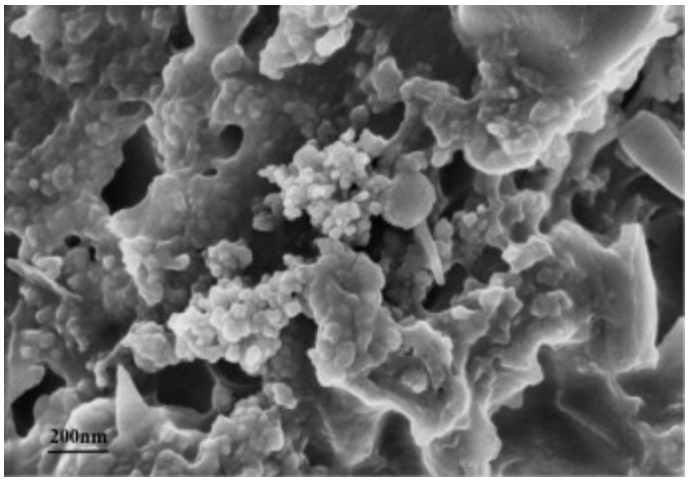

Fig. S2 The morphology of AC as analysed by SEM.

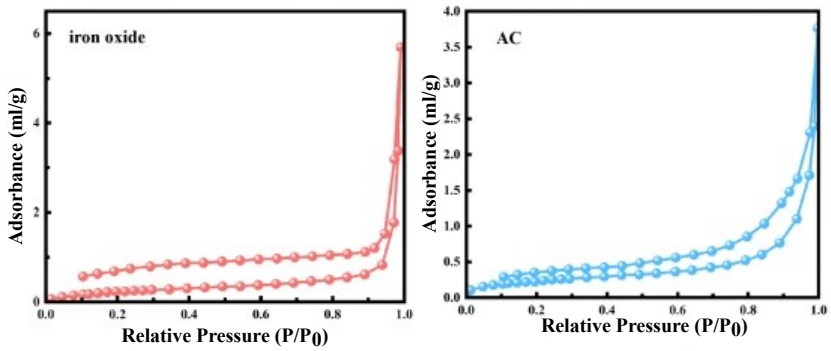

Fig. S3 N_2 adsorption-desorption isotherms of iron oxide and AC.

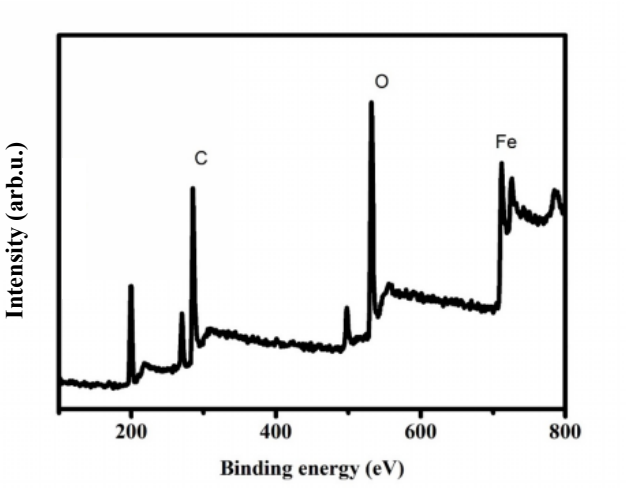

Fig. S4 The XPS spectrum of the FexO/AC composite.